

# Fast Implementations of the Kalman–Bucy Filter for Satellite Data Assimilation

Amir Asif, *Senior Member, IEEE*

**Abstract**—We present practical data assimilation algorithms based on the Kalman–Bucy filter (KbF) for combining satellite altimetry data with the nonlinear ocean circulation models. Data assimilation in such applications is computationally challenging because of the large dimensions of the state fields. Compared with the direct KbF, our KbF implementations provide computational savings of two orders of the magnitude of the linear dimension of the state field. We run twin experiments by interfacing our data assimilation algorithms with the NLOM, a nonlinear ocean circulation model developed at the Naval Research Laboratory.

**Index Terms**—Block-banded matrices, data assimilation, Kalman–Bucy filter, multidimensional signal processing.

## I. INTRODUCTION

ESTIMATING the state of the ocean fields (e.g., the sea surface height and ocean velocity components) is a key issue in physical oceanography. Direct application of the Kalman–Bucy filter (KbF) in such data assimilation [1]–[5] problems is difficult for two reasons. First, the state equations are nonlinear, and the resulting KbF is nonrigorous. Second, the KbF involves formidable computational requirements in inverting and storing the covariance matrices such that its application is limited to relatively simple oceanographic models.

### A. Main Contributions

The focus of the letter is as follows.

- 1) To develop practical implementations of the local KbF [2] for *nonlinear* ocean circulation models. While [2] is limited to dynamical models arising from the discretization of linear partial differential equations (pdes), we extend the work to nonlinear models such as the Navy layered ocean model (NLOM), [6]. A second difference arises due to the structure of the state matrices. While the state matrices in [2] are block banded, the state matrices in the NLOM are full matrices. However, the blocks that constitute the state matrices are subblock banded so, the local KbF is applied at the subblock level to the NLOM.
- 2) To generalize the local KbF to an  $M$ -block banded approximation. Asif and Moura [2] applies a tridiagonal ( $M = 1$ ) block banded approximation to the inverse of the error covariance matrix. In this letter, we generalize the result to an  $M$ -block banded approximation.

Manuscript received March 13, 2003; revised May 1, 2003. This work was supported by the Natural Sciences and Engineering Research Council of Canada (NSERC) under Grant 228415-03. The associate editor coordinating the review of this manuscript and approving it for publication was Prof. Janusz Konrad.

A. Asif is with the Department of Computer Science, York University, Toronto, ON M3J 1P3, Canada (e-mail: asif@cs.yorku.ca).

Digital Object Identifier 10.1109/LSP.2003.821672

- 3) To apply the KbF-based data assimilation to the NLOM and illustrate the improvement in the ocean prediction resulting from the data assimilation algorithm.

The letter is organized as follows. Section II describes the dynamical models used in ocean circulation. Section III presents our data assimilation algorithms. Twin experiments are included in Section IV. Section V concludes the letter.

## II. DYNAMICAL MODELS

For compactness, the primitive pdes are expressed as

$$\frac{\partial \psi}{\partial t} = \mathcal{D}\psi + \mathcal{F}, \quad \mathcal{D} = \sum_{n_1, n_2, n_3} \left( \frac{\partial}{\partial \theta} \frac{\partial}{\partial \phi} a_{n_1 n_2 n_3}(\theta, \phi) \right) \quad (1)$$

where  $\psi$  represents multiple ( $q$ ) fields like sea surface height (SSH)  $h$ , and the latitudinal and longitudinal velocity components ( $u, v$ ). The operator  $\mathcal{D}$  is the nonlinear pde operator,  $\theta$  and  $\phi$  are the latitudinal and longitudinal coordinates, and  $\mathcal{F}$  incorporates the wind forcings. See [6] for details.

In a numerical simulation, the ocean domain constrained by the latitudinal and longitudinal boundaries is discretized into an  $(I \times J)$  grid with  $L$  layers. A set of finite-difference equations obtained by discretizing (1) using the staggered C-grid leap frog finite-difference scheme, computes the ocean circulation fields  $h, u,$  and  $v$  for each layer. In our derivations, a row of each of the discretized field in layer  $\ell$  is first mapped into a  $(J \times 1)$  random vector, and these are stacked one on the top of the other to form a  $(qIJ \times 1)$  vector, such as

$$\Psi^{(\ell)} = \left[ \underbrace{h_1^T, u_1^T, v_1^T}_{\Psi_1^{(\ell)}}, \underbrace{h_2^T, u_2^T, v_2^T}_{\Psi_2^{(\ell)}}, \dots, \underbrace{h_I^T, u_I^T, v_I^T}_{\Psi_I^{(\ell)}} \right]^T \quad (2)$$

for  $q = 3$  and where  $h_i = [h_{i1}, h_{i2}, \dots, h_{iJ}]^T$ , for  $1 \leq i \leq I$ . A similar notation is used for the field vector  $u_i$  and  $v_i$ . The superscript  $\ell$  denotes the number of the layer under consideration, ( $1 \leq \ell \leq L$ ). The state vector  $\Psi$  consists of field vectors  $\Psi^{(\ell)}$  for each layer stacked together in the order of the depth. Additional terms that provide coupling between the vertical layers are also included in the dynamical model of (1). The time step is derived from the Courant–Friedrich–Lewy (CFL) conditions.

It is interesting to note the structure in the covariance matrix  $\mathcal{P} = \{P^{(\ell_1 \ell_2)}\}$ , ( $1 \leq \ell_1, \ell_2 \leq L$ ), with blocks

$$P^{(\ell_1 \ell_2)} = \begin{bmatrix} P_{11}^{(\ell_1 \ell_2)} & \cdot & P_{1I}^{(\ell_1 \ell_2)} \\ \cdot & \ddots & \cdot \\ P_{I1}^{(\ell_1 \ell_2)} & \cdot & P_{II}^{(\ell_1 \ell_2)} \end{bmatrix} \quad (3)$$

of dimension  $(qIJ \times qIJ)$  denoting the covariance between field vectors  $\Psi^{(\ell_1)}$  and  $\Psi^{(\ell_2)}$  for layers  $\ell_1$  and  $\ell_2$  of the ocean field. The covariance blocks  $P^{(\ell_1 \ell_2)}$  are further expanded in terms of  $(qJ \times qJ)$  subblocks  $P_{ij}^{(\ell_1 \ell_2)}$  representing the covariance between the  $q$  ocean fields of row  $i$  in layer  $\ell_1$  and the corresponding fields of row  $j$  in layer  $\ell_2$ .

#### A. Satellite Measurements

The satellite tracks are curved, so data  $\mathcal{Y}$  are available on a few sites along  $N$  adjacent rows,  $m, \dots, p$ , in the top layer ( $\ell = 1$ )

$$\underbrace{\begin{bmatrix} \mathcal{Y}_m^{(1)}(k+1) \\ \vdots \\ \mathcal{Y}_p^{(1)}(k+1) \end{bmatrix}}_{\mathcal{Y}^{(k+1)}} = \underbrace{\begin{bmatrix} \Theta(k+1) & \mathbf{0} & \dots & \mathbf{0} \end{bmatrix}}_{\mathcal{H}^{(k+1)}} \Psi(k+1) + \xi \quad (4)$$

with

$$\Theta(k+1) = \begin{bmatrix} \mathbf{0} & \dots & \mathbf{0} & \theta_m & \mathbf{0} & \dots & \mathbf{0} & \mathbf{0} & \mathbf{0} & \dots & \mathbf{0} \\ \vdots & \vdots & \vdots & \vdots & \vdots & \vdots & \vdots & \vdots & \vdots & \vdots & \vdots \\ \mathbf{0} & \dots & \mathbf{0} & \mathbf{0} & \mathbf{0} & \dots & \mathbf{0} & \theta_p & \mathbf{0} & \dots & \mathbf{0} \end{bmatrix}. \quad (5)$$

For a total of  $L$  vertical layers, the observation matrix  $\mathcal{H}^{(k+1)}$  is of dimensions  $(qNJ \times qLIJ)$  and is highly sparse. The constituent blocks  $\theta_i$ 's of  $\Theta$  are also sparse since the satellite provides data only on the SSH,  $h$ . The velocity components ( $u, v$ ) are not observed. The variable  $\xi$  in (4) represents the measurement noise, assumed Gaussian and  $k$  is the time index.

### III. EXTENDED KBF

To apply the KBf for data assimilation, the state model is linearized by approximating (1) with the shallow water model

$$\frac{\partial h^{(\ell)}}{\partial t} + \frac{H^{(\ell)}}{a \cos \theta} \left[ \frac{\partial u^{(\ell)}}{\partial \phi} + \frac{\partial (v^{(\ell)} \cos \theta)}{\partial \theta} \right] = 0 \quad (6)$$

$$\frac{\partial u^{(\ell)}}{\partial t} - k_1 v^{(\ell)} + \sum_{\tau=1}^L \frac{h^{(\ell)} G^{(\ell \tau)}}{a \cos \theta} \frac{\partial (h^{(\tau)} - H^{(\tau)})}{\partial \phi} = F_\phi \quad (7)$$

$$\frac{\partial v^{(\ell)}}{\partial t} + k_1 u^{(\ell)} + \sum_{\tau=1}^L \frac{h^{(\ell)} G^{(\ell \tau)}}{a} \frac{\partial (h^{(\tau)} - H^{(\tau)})}{\partial \theta} = F_\theta \quad (8)$$

where  $k_1$  is the Coriolis constant given by  $2\Omega \sin \theta$ ,  $\Omega$  being the Coriolis parameter. The term  $H^{(\ell)}$  denotes the thickness of layer  $\ell$ , ( $F_\phi, F_\theta$ ) are the longitudinal and latitudinal components of the forcing term  $F$ , and  $G^{(\ell \tau)}$  is the reduced gravity parameter. Discretizing (6)–(8) with the staggered C-grid leap frog finite-difference scheme, followed by a real-time Taylor approximation of the nonlinear terms, gives the state equation

$$\Psi(k+1) = \mathcal{A}(k)\Psi(k) + \mathcal{C}(k)W(k) \quad (9)$$

where the state matrices  $\mathcal{A}$  and  $\mathcal{C}$  are full matrices that are partitioned in terms of the time varying blocks,  $\mathcal{A} = \{A^{(\ell_1 \ell_2)}\}$  and  $\mathcal{C} = \{C^{(\ell_1 \ell_2)}\}$ , for  $(1 \leq \ell_1, \ell_2 \leq L)$ . The blocks  $A^{(\ell_1 \ell_2)}$  and  $C^{(\ell_1 \ell_2)}$  have the same dimensions as the covariance blocks  $P^{(\ell_1 \ell_2)}$  but are highly structured with  $A^{(\ell_1 \ell_2)}$  being  $M_1$ -block

banded and  $B^{(\ell_1 \ell_2)}$  being  $M_2$ -block banded. The banded structure arises from the local field interactions resulting from the discretization of the pdes (6)–(8). We emphasize that the linear shallow water approximation (9) is only used to update the forecast error covariance matrix in the KBf. The nonlinear primitive equations (1) predict the model state.

#### A. Data Assimilation Algorithm

Our data assimilation algorithm applies the  $M$ -block banded approximation to the inverse of the block  $P^{(\ell_1 \ell_2)}$  based on Theorem 1 [7]. The algorithm is outlined in Section III-B.

*Theorem 1:* Given blocks  $\{P_{ij}^{(\ell_1 \ell_2)}\}$  on the first  $M$ -subblock diagonals of  $P^{(\ell_1 \ell_2)} = (B^{(\ell_1 \ell_2)})^{-1}$ ,  $B^{(\ell_1 \ell_2)}$  being  $M$ -subblock banded, the subblocks outside the  $M$ -subblock diagonals in  $P^{(\ell_1 \ell_2)}$  are

$$P_{ij} = \begin{bmatrix} P_{ii+1}^{(\ell_1 \ell_2)} & \dots & P_{ii+M}^{(\ell_1 \ell_2)} \end{bmatrix} \cdot \begin{bmatrix} P_{i+1i+1}^{(\ell_1 \ell_2)} & \dots & P_{i+1i+M}^{(\ell_1 \ell_2)} \\ \vdots & \ddots & \vdots \\ P_{i+Mi+1}^{(\ell_1 \ell_2)} & \dots & P_{i+Mi+M}^{(\ell_1 \ell_2)} \end{bmatrix}^{-1} \begin{bmatrix} P_{i+1j}^{(\ell_1 \ell_2)} \\ \vdots \\ P_{i+Mj}^{(\ell_1 \ell_2)} \end{bmatrix} \quad (10)$$

for  $1 \leq i < (I - M)$  and  $(i + M) < j \leq I$ . ■

#### B. Local KBf

Initial conditions:  $\hat{\Psi}(0|0)$ ,  $\mathcal{P}(0|0)$ , state and observation covariance ( $\mathcal{Q}, \mathcal{R}$ ) at  $k = 0$ .

- Step 1) Update the field  $\hat{\Psi}(k+1|k)$  using the NLOM, (1).
- Step 2) Update the *a priori* error covariance. In terms of blocks  $\mathcal{A} = \{A^{(\ell_1 \ell_2)}\}$ ,  $\mathcal{C} = \{C^{(\ell_1 \ell_2)}\}$ ,  $\mathcal{P} = \{P^{(\ell_1 \ell_2)}\}$ , and  $\mathcal{Q} = \{Q^{(\ell_1 \ell_2)}\}$ , the error covariance is

$$P^{(\ell_1 \ell_2)}(k+1|k) = \sum_{\tau_2=1}^L \left( \sum_{\tau_1=1}^L A^{(\ell_1 \tau_1)}(k) P^{(\tau_1 \tau_2)}(k|k) \right) \left( A^{(\ell_2 \tau_2)}(k) \right)^T + \sum_{\tau_2=1}^L \left( \sum_{\tau_1=1}^L C^{(\ell_1 \tau_1)}(k) Q^{(\tau_1 \tau_2)}(k) \right) \left( C^{(\ell_2 \tau_2)}(k) \right)^T \quad (11)$$

for  $(1 \leq \ell_1, \ell_2 \leq L)$ . Equation (11) includes sum of several product terms  $A^{(**)} P^{(**)}(k|k) (A^{(**)})^T$ , each expressed in terms of subblocks as

$$\begin{aligned} & \left[ A_1^{(**)} P_{i-1j-1}^{(**)} + A_2^{(**)} P_{ij-1}^{(**)} + A_3^{(**)} P_{i+1j-1}^{(**)} \right] \left( A_1^{(**)} \right)^T \\ & + \left[ A_1^{(**)} P_{i-1j}^{(**)} + A_2^{(**)} P_{ij}^{(**)} + A_3^{(**)} P_{i+1j}^{(**)} \right] \left( A_2^{(**)} \right)^T \\ & + \left[ A_1^{(**)} P_{i-1j+1}^{(**)} + A_2^{(**)} P_{ij+1}^{(**)} + A_3^{(**)} P_{i+1j+1}^{(**)} \right] \left( A_3^{(**)} \right)^T. \end{aligned}$$

where the block  $A^{(\ell_1 \ell_2)}$  is assumed to be tridiagonal subblock banded,<sup>1</sup> ( $M_1 = 1$ ), with subblocks  $A_1^{(\ell_1 \ell_2)}$ ,  $A_2^{(\ell_1 \ell_2)}$ , and  $A_3^{(\ell_1 \ell_2)}$  on its lower, main, and upper subblock diagonals. The  $M$ -subblock banded

<sup>1</sup>The discussion presented here is generalizable to the  $M_1$ -subblock banded case for the state matrix  $\mathcal{A}$ .

approximation on block  $P^{(\ell_1 \ell_2)}(k+1|k)$  implies that we update only the main and the first  $M$  upper sub-block diagonals in each such block. An update of  $P_{ij}^{(\ell_1 \ell_2)}(k+1|k)$ ,  $|j-i| \leq M$ , requires subblocks

$$P_{ij}^{(\ell_1 \ell_2)}(k|k), \quad \text{for } |j-i| \leq (M+2) \quad (12)$$

from the last iteration of the KBf. Of the required subblocks  $P_{ij}^{(\ell_1 \ell_2)}(k|k)$  in (12), the subblocks on the first  $M$  subblock diagonals are obtained from the previous iteration. The remaining subblocks on diagonals  $(M+1)$  and  $(M+2)$  are computed from the first  $M$ -subblock diagonals using Theorem 1. A similar procedure approximates  $Q^{(\ell_1 \ell_2)}$ .

Step 3) Compute the Kalman gain expressed as

$$K^{(\ell)}(k+1) = P^{(\ell)}(k+1|k)\Theta^T(k+1) \cdot \left[ \Theta(k+1)P^{(11)}(k+1|k)\Theta^T(k+1) + R^{(11)}(k+1) \right]^{-1} \quad (13)$$

where  $K^{(\ell)}$  is the  $(qIJ \times qNJ)$  Kalman gain for layer  $\ell$ ,  $(1 \leq \ell \leq L)$ . At the subblock level, (13) is

$$K_i^{(\ell)}(k+1) = \begin{bmatrix} P_{1m}^{(\ell 1)} \theta_m^T & \dots & P_{1p}^{(\ell 1)} \theta_p^T \\ \left( \theta_m P_{mm}^{(11)} \theta_m^T + R_{mm}^{(11)} \right) & \cdot & \theta_m P_{mp}^{(11)} \theta_p^T \\ \vdots & \ddots & \vdots \\ \theta_p P_{pm}^{(11)} \theta_m^T & \cdot & \left( \theta_p P_{pp}^{(11)} \theta_p^T + R_{pp}^{(11)} \right) \end{bmatrix} \quad (14)$$

where  $K_i^{(\ell)}(k+1)$  is a  $(qJ \times qNJ)$  subblock that represents the Kalman gain for row  $i$  of layer  $\ell$ ,  $(1 \leq i \leq I)$  and  $(1 \leq \ell \leq L)$ . Updating the Kalman gain  $K_i^{(\ell)}(k+1)$  requires a few subblocks  $P_{ij}^{(\ell_1 \ell_2)}$  from outside the  $M$ -subblock diagonals in block  $P^{(\ell_1 \ell_2)}$ . These are computed from the subblocks within the  $M$ -subblock diagonal of  $P^{(\ell_1 \ell_2)}$  using Theorem 1.

Step 4) Compute the predicted estimate from the measurements. At the block level

$$\widehat{\Psi}^{(\ell)}(k+1|k+1) = \widehat{\Psi}^{(\ell)}(k+1|k) + K^{(\ell)}(k+1) \cdot \left[ \mathcal{Y}^{(1)}(k+1) - \Theta(k+1)\widehat{\Psi}_m^{(1)}(k+1|k) \right] \quad (15)$$

for  $(1 \leq \ell \leq L)$ . Expanding further to the subblock level gives

$$\widehat{\Psi}_i^{(\ell)}(k+1|k+1) = \widehat{\Psi}_i^{(\ell)}(k+1|k) + K_i^{(\ell)}(k+1) \begin{bmatrix} \mathcal{Y}_m^{(1)}(k+1) - \theta_m \widehat{\Psi}_m^{(1)}(k+1|k) \\ \vdots \\ \mathcal{Y}_p^{(1)}(k+1) - \theta_p \widehat{\Psi}_p^{(1)}(k+1|k) \end{bmatrix} \quad (16)$$

for  $(1 \leq i \leq I)$  and  $(1 \leq \ell \leq L)$ . The ocean field  $\Psi$  is updated one row at a time.

Step 5) Compute the *a posteriori* covariance matrix using

$$P^{(\ell_1 \ell_2)}(k+1|k+1) = P^{(\ell_1 \ell_2)}(k+1|k) - K^{(\ell_1)}(k+1)\Theta(k+1)P^{(1 \ell_2)}(k+1|k) \quad (17)$$

for  $(1 \leq \ell_1, \ell_2 \leq L)$ . Simplifying (17) gives

$$P_{ij}^{(\ell_1 \ell_2)}(k+1|k+1) = P_{ij}^{(\ell_1 \ell_2)}(k+1|k) - K_1^{(\ell_1)}(k+1) \begin{bmatrix} \theta_m P_{mj}^{(1 \ell_2)}(k+1|k) \\ \vdots \\ \theta_p P_{pj}^{(1 \ell_2)}(k+1|k) \end{bmatrix} \quad (18)$$

for  $(1 \leq i, j \leq I)$ ,  $|j-i| \leq M$ , and  $(1 \leq \ell_1, \ell_2 \leq L)$ . Equation (18) is updated for  $P_{ij}^{(\ell_1 \ell_2)}(k+1|k+1)$  that lie within the first  $M$  subblock diagonals. A few subblocks  $P_{ij}^{(\ell_1 \ell_2)}(k+1|k)$  in (18) lie outside the first  $M$  subblock diagonals and are computed from the  $M$  subblock diagonal blocks using Theorem 1.

Step 6) Increment  $k$  by 1 and go back to step 1).

#### IV. TWIN EXPERIMENT

An equatorial channel of the Pacific Ocean within the latitudes of  $\pm 20^\circ$  is simulated. The longitude varies from  $306^\circ$  to  $374^\circ$ . Twin experiments on a  $1/4^\circ$ ,  $2(1/2)$  layer hydrodynamic NLOM with analytical winds ( $F_\phi$ ,  $F_\theta$ ) are performed. The dimension of the state vector is roughly of  $O(10^6)$ .

- *Deterministic setup*: runs the NLOM with analytical winds to propagate the deterministic components. Such theoretical estimates are often used by oceanographers to model ocean circulation in various regions of the ocean.
- *Real-world setup*: extends the deterministic setup by adding White Gaussian noise with a SNR of 12 dB to the wind forcings ( $F_\phi$ ,  $F_\theta$ ). The noise defines the state covariance  $\mathcal{Q}$ .

The two simulations described above are run for a simulated period of six months.

- *Data Assimilation*: The SSH,  $h^{(1)}$ , of the real-world setup is assimilated as pseudodata, (4), into the deterministic setup to estimate the results of the real world. Gaussian noise of 10 dB is added to the altimetry observations,  $h$ . The covariance  $\mathcal{R}$  is defined by the observation noise.
- *Results*: In our data assimilation experiment, we use a pentadiagonal subblock approximation ( $M=2$ ) in the local KBf to assimilate the satellite data in the NLOM. Figs. 1–3 show estimates of the SSH for the top layer from the three setups described earlier, at day 36 after three satellite repeat cycles. A visual comparison of the figures illustrates that the SSH image associated with the satellite scanned sparse data is a better estimate of the actual ocean state condition, in our case, the real-world run, than the field predicted with no data assimilation. The latter is a low-pass version of the actual SSH. The data-assimilated SSH incorporates the finer details like the eddies, as, for example, the valleys and the peaks in Fig. 1 are well reproduced in Fig. 3 but are smoothed out in Fig. 2. In Fig. 4, a quantitative comparison based on the mean square error (MSE) is performed. The relative MSE (RMSE) plotted in Fig. 4 is defined as the ratio of the MSE of the data-assimilated run to the MSE of the deterministic run. The region below ordinate ( $y=1$ ) represents improvement made by the data-assimilated run. With time, the RMSEs for both

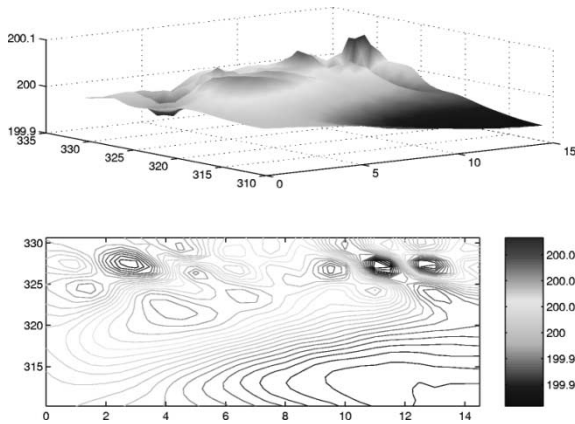


Fig. 1. Mesh and contour plots of the sea surface height (SSH) in meters for the top layer from the *real-world setup*.

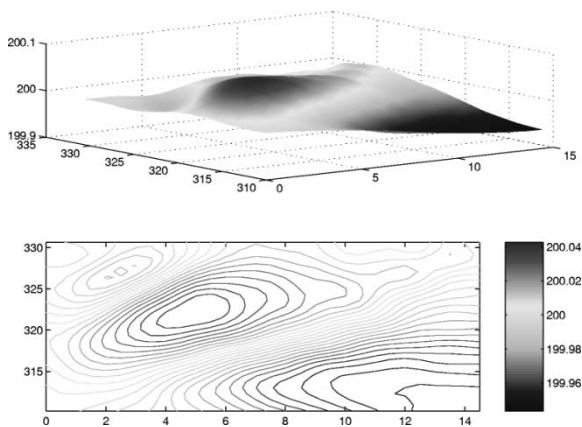


Fig. 2. Mesh and contour plots of the SSH of the top layer from the *deterministic setup*. The plots do not capture the finer details like the eddies, the troughs, and the crests of Fig. 1.

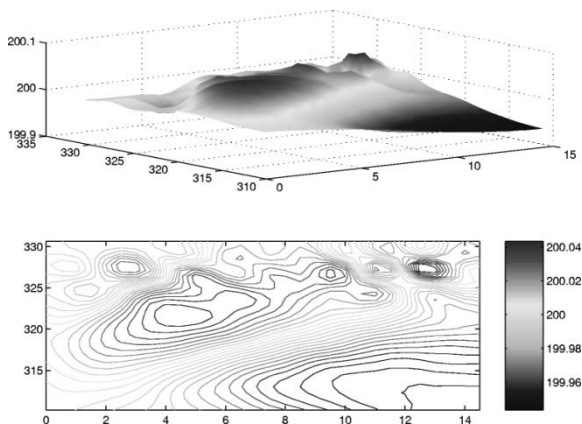


Fig. 3. Mesh and contour plots of the SSH of the top layer from the *data assimilation setup*. These images illustrate that the data-assimilated SSHs are a better estimate of the real-world run. See Fig. 1.

layers drop suggesting improvements with data assimilation. The improvement is higher, roughly 25% after 36

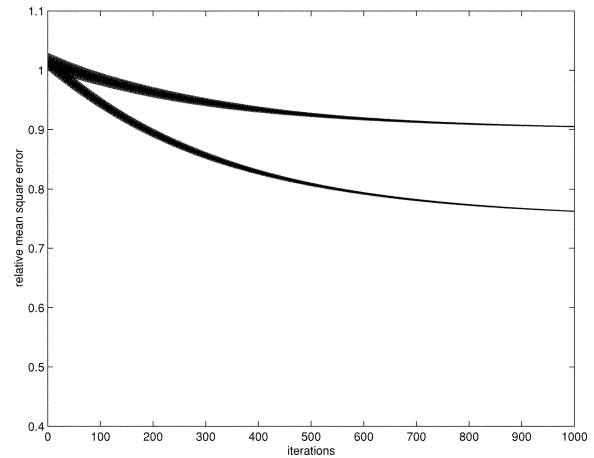


Fig. 4. RMSE of the SSH of the top and the lower layer. The lower curve is the RMSE for the surface layer, while the upper curve is the RMSE for the second lower layer.

days, for the upper layer for which altimetry data is available. No data are assimilated for layer 2, yet we see an improvement of about 10%. Our Kbf implementation successfully correlates the two layers and projects the surface information into the lower layer.

## V. SUMMARY

Assimilation of the altimetry data has been investigated for the NLOM. We use a Kbf implementation that couples dynamic linearization with an  $M$ -block banded approximation to the inverse of the error covariance blocks. Simulation with the NLOM shows significant improvement in the prediction of ocean fields. The Kbf implementation successfully projects the surface information into the subsurface layers.

## REFERENCES

- [1] T. M. Chin, A. J. Mariano, and E. P. Chassignet, "Spatial regression with Markov random fields for Kalman filter approximation in least squares solution of oceanic data assimilation problems," *J. Geophys. Res.*, vol. 104, pp. 7991–8014, 1999.
- [2] A. Asif and J. M. F. Moura, "Data assimilation in large time varying multidimensional fields," *IEEE Trans. Image Processing*, vol. 8, Nov. 1999.
- [3] D. T. Pham, J. Verron, and M. C. Roubaud, "A singular extended Kalman filter for data assimilation in oceanography," *J. Marine Syst.*, vol. 16, pp. 323–340, 1998.
- [4] R. N. Miller and M. A. Cane, "Tropical data assimilation: Theoretical concepts," in *Modern Approaches to Data Assimilation in Ocean Modeling*, P. M. Rizzoli, Ed. New York: Elsevier, 1996, pp. 207–233.
- [5] I. Fukumori and P. Malanotte-Rizzoli, "An approximate Kalman filter for ocean data assimilation: An example with an idealized Gulf Stream Model," *J. Geophys. Res.*, vol. 100, pp. 6777–6793, 1995.
- [6] D. R. Moore and A. J. Wallcraft, "Formulation of the NRL layered ocean model in spherical coordinates," Nav. Res. Lab., Stennis Space Center, MS, Tech. Rep. CR 7323-96-0005, 1995.
- [7] A. Asif and J. M. F. Moura, "Block matrices with  $L$ -block banded inverse: Inversion algorithms," *IEEE Trans. Signal Processing*, 2003, submitted for publication.